Journal of Marine Science and Application
https://doi.org/10.1007/s11804-018-0038-0

RESEARCH ARTICLE

Time-Domain Analysis of the Relative Motions Between Side-by-Side FLNG and LNGC Under Oblique Waves

Ke Zhou [1] · Zhiqiang Hu [2] · Dongya Zhao [1]

Received: 26 July 2017 / Accepted: 8 May 2018

Abstract
Strong hydrodynamic interactions during the side-by-side offloading operation between floating liquefied natural gas (FLNG) and liquefied natural gas carrier (LNGC) can induce high risks of collision. The weather vane effect of a single-point mooring system normally results in the satisfactory hydrodynamic performance of the side-by-side configuration in head seas. Nevertheless, the changes in wave directions in real sea conditions can significantly influence the relative motions. This article studies the relative motions of the side-by-side system by using the theoretical analysis method and the numerical calculation method. Based on the three-dimensional potential theory modified by artificial damping-lid method, the frequency-domain hydrodynamic coefficients can be improved to calculate the retardation functions for the multi-body problem. An in-house code is then developed to perform the time-domain simulation of two vessels, through which the relative motions are subsequently obtained. A range of oblique waves are chosen for the extensive calculation of relative motions between the two vessels, which are further analyzed in terms of the phase shift of motion responses induced by specific resonant wave patterns. Investigation results show that wave directions have a significant influence on the relative sway, roll, and yaw motions. Under the circumstance that the absolute phase shift between the roll motions of two vessels approaches 180°, stronger relative motions are induced when LNGC is on the weather side. Moreover, the gap water resonances at high frequencies tend to cause the dangerous opposed oscillation of two vessels in the sway and yaw modes, whereas FLNG reduces the gap water resonances and relative motions when located on the weather side.

Keywords Floating liquefied natural gas (FLNG) · Multi-body system · Time-domain simulation · Oblique waves · Relative motion · Gap resonance · Shielding effect

1 Introduction

The floating liquefied natural gas (FLNG) system offers great safety as well as economic and environmental advantages in the development of marginal gas fields by means of liquefying the natural gas on the production barge and offloading it to a shuttle carrier. Nevertheless, due to the cryogenic nature of liquefied natural gas (LNG), conventional floating hoses for tandem-offloading are too long to be used in LNG offloading operation. LNG loading arms, as a substitute for hoses, requires the side-by-side offloading configuration, whereas the relative motions during side-by-side offloading can induce high tensions in the mooring lines between the floaters and large angles in the offloading arms (Soares et al. 2015). In addition, the risks of collision may increase due to large relative motions induced by the strong hydrodynamic interactions between the two nearby floaters, especially under oblique waves. Hence, the investigation of relative motions between side-by-side FLNG and LNGC under various oblique waves is very important in ensuring the safety of the system.

For this multi-body problem in the frequency domain, extensive works have been carried out toward the simulation of hydrodynamic interactions between bodies and the viscous influence of flow in the gap region. On the basis of the three-dimensional (3D) potential flow theory, Oortmerssen (1979) calculated the motion responses of the closely arranged cylinder and barge in head seas. Fang and Chen (2002)

This study is supported by the China National Scientific and Technology Major Project (2016ZX05028-002-004).

✉ Zhiqiang Hu
zhiqiang.hu@ncl.ac.uk

[1] State Key Laboratory of Ocean Engineering, Shanghai Jiao Tong University, Shanghai 200240, China

[2] School of Engineering, Newcastle University, Newcastle upon Tyne NE1 7RU, UK

Published online: 23 October 2018

investigated the relative motions and gap water elevations between parallel hulls and validated the accuracy of the 3D panel model over the two-dimensional (2D) strip model. Choi and Hong (2002) adopted the higher order boundary element method to study motion responses and second-order forces of the multi-body FPSO and shuttle tankers operating in side-by-side offloading. Due to the basic assumption of potential flow that fluids are treated as inviscid and irrotational, the strong viscous effect in between the hulls is difficult to simulate without any modification of the classic potential flow theory. Therefore, many scholars have attempted to account for the viscous effect. An early method developed by Huijsmans et al. (2001), the rigid-lid method, aimed to eliminate any vertical free-surface motions. Another method involved incorporating a damping coefficient into the potential flow to adjust the energy dissipation artificially, which is equivalent to the energy dissipation generated from vortex shedding and viscous drag forces on hulls. Chen (2005) proposed the damping-lid method by introducing a dissipation term ("epsilon") to the free-surface condition. This scheme has been widely used and validated by later studies (Fournier et al. 2006; Pauw et al. 2007; Xu et al. 2015; Sclavounos and Ma 2018) in the study of side-by-side problem in terms of the motion responses, gap free-surface elevations, and second-order forces. The gap resonance and higher harmonics in the gap region were also experimentally studied by Zhao et al. (2017).

Meanwhile, the time-domain simulation of side-by-side vessels has been carried out by many scholars to investigate the hydrodynamic interactions based on the impulse-response-function method proposed by Cummins (1962). For example, Buchner et al. (2001) calculated the time traces of ship motions in the side-by-side configuration based on the rigid-lid method modification. They used a fully coupled method that included all cross-diagonal terms in the matrix for greater accuracy. The Rankine panel method was also used by Kim et al. (2008) to investigate the global motions and relative motions of adjacent floaters under oblique waves in the time domain. Watai et al. (2015) applied the damping-lid method onto the confined area between vessels, and studied the seakeeping of side-by-side floaters in the time domain to determine the damping-lid helps to facilitate the convergence of the time-domain computation.

Although many studies have been carried out to investigate the side-by-side configuration, few of them focused on the strong hydrodynamic interactions under oblique waves, which aggravate the risks of collision. Thus, the aim of the present study is to investigate the influence of wave directions on the relative motions of this asymmetric multi-body system. First, a numerical simulation based on an in-house code in time domain is implemented. The changes of relative motions under a range of wave directions are studied, and the dangers induced by transient effect are captured in time-domain analysis. For the resonances of relative motions, phase shifts between motions of two vessels are considered, and their relations with patterns of gap free-surface resonances are further elucidated.

2 Mathematical Formulation

2.1 Coordinate Systems

To describe the motions and hydrodynamic forces of the hulls, three coordinates must be established: the respective body systems fixed at the mean position of each body with the subscript of A or B to represent the FLNG and LNGC, respectively, and a global coordinate system fixed in the gap center (Fig. 1). The origins of the three coordinates are placed on the undisturbed free surface, and as can be seen, the x-axis positively points toward the ship bow, while the z-axis points vertically upwards.

2.2 Frequency-Domain Equations

Assuming the ideal fluid is inviscid and incompressible, the velocity potential Φ is introduced to describe the fluid domain, which satisfies the Laplace equation given by the following:

$$\nabla^2\Phi = 0 \tag{1}$$

The linearized boundary value problem can be derived after the expansion of the velocity potential and other physical quantities with respect to the mean wet surface in still water. Due to the principle of linear superposition for the velocity potential, the total periodic velocity potential in form of sinusoidal oscillation can be expressed as follows:

$$\Phi(x,y,z,t) = \mathrm{Re}\left\{\left[\xi(\phi_I+\phi_D)+\sum_{i=1}^{2}\sum_{j=1}^{6}x_j^{(i)}\phi_j^{(i)}\right]\mathrm{e}^{-i\omega t}\right\} \tag{2}$$

where ξ represents the wave amplitude; $x_j^{(i)}$ and $\phi_j^{(i)}$ $(i=1,2;j=1,2,\ldots6)$ are the complex amplitude and the radiation potential induced by the forced motion of the jth mode for body i, respectively; ϕ_I is the incident potential; and ϕ_D is the diffraction potential induced by the presence of bodies in waves.

The hydrodynamic interactions among hulls arise from the consideration of the exciting force induced by the radiation wave from the other body's oscillation. Therefore, the fluid domain should be taken as a whole system, and the 12 generalized modes of the 2 floating bodies are fully coupled. Nevertheless, the multi-body problem is fundamentally an extension of the single-body boundary value problem; hence, only the differences in governing equations are briefly summarized. Details are elaborated in previous studies by Xu et al. (2015).

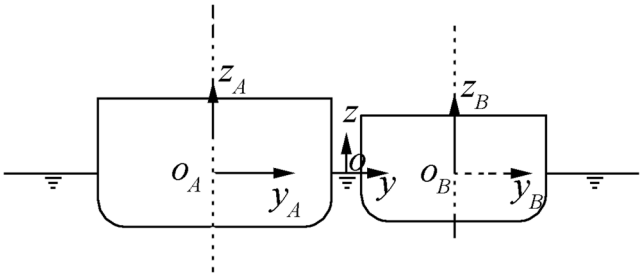

Fig. 1 Definition of the coordinate systems

The difference in the body boundary condition S_B for the new one consists of both body surfaces, and is expressed as follows:

$$S_B = \sum_{i=1}^{2} S_B^{(i)}, i = 1, 2 \tag{3}$$

The corresponding body conditions in the radiation problem are given by the following:

$$\frac{\partial}{\partial n}\phi_j^{(m)} = \delta_{mn} n_j^{(n)}, (m, n = 1, 2) \tag{4}$$

$$\delta_{mn} = 1(m = n) \text{ or } \delta_{mn} = 0(m \neq n) \tag{5}$$

where $\phi_j^{(m)}$ is the normalized radiation potential of body m under jth mode and δ_{mn} is the Kronecker symbol. For body1, $(n_{1(1)}, n_{2(1)}, n_{3(1)}) = n$, $(n_{4(1)}, n_{5(1)}, n_{6(1)}) = r \times n$, where n stands for the unit surface normal vector and r for the radius vector at any point in the body system.

When two parallel floaters are located close to each other, the hydrodynamic coefficients are always overestimated due to the negligence of strong viscous effect in the gap zone. The damping-lid method (Chen 2005) is presented to address this issue. The traditional inviscid potential flow is modified by introducing a fictitious force that is dependent on the fluid velocity in the momentum equation given by the following:

$$f_{\mathrm{dmp}} = -\mu V \tag{6}$$

where V is the velocity of water particles and μ is defined as a damping factor. Given that this fictitious force does not introduce any vorticity, by incorporating the viscous effect of fluid motion, the existence of velocity potential is ensured. The Bernoulli equation can be expressed as follows:

$$\frac{P}{\rho} + gz + \frac{\partial \Phi}{\partial t} + \frac{\nabla\Phi \cdot \nabla\Phi}{2} + \mu\Phi = 0 \tag{7}$$

where ρ is the water density and g is the acceleration of gravity. Ignoring the second-order item, the first-order wave elevation can be expressed as follows:

$$\eta = -\frac{1}{g}\left(\frac{\partial \Phi}{\partial t} + \mu\Phi\right) \tag{8}$$

For the first-order boundary value problem, the conventional free-surface condition can be modified as follows:

$$-(1 + i\varepsilon)\omega^2\phi_m + g\frac{\partial}{\partial z}\phi_m = 0, \frac{\mu}{\omega} = \varepsilon \tag{9}$$

where ε represents the artificial damping coefficient ranging between 0 and 1. When $\varepsilon = 0$, this boundary condition degrades into the conventional linearized free-surface condition, and when $\varepsilon = 1$, no wavy free surface is allowed; hence, it turns into a rigid lid.

2.3 Time-Domain Calculation

Based on the reasonable frequency-domain results, the motion equation in time domain can be written as follows according to Cumming's theory:

$$[M + a(\infty)]\left\{\ddot{\xi}(t)\right\} + \int_0^t [h(t-\tau)]\left\{\ddot{\xi}(t)\right\}d\tau + C_{\mathrm{vis}}\left\{\ddot{\xi}(t)\right\} + K\{\xi(t)\} = F(t) \tag{10}$$

where M and $a(\infty)$ are the generalized mass matrix and added mass matrix at infinity frequency, respectively; $\xi(t)$ stands for the integrated displacement vector of two vessels; K refers to the restoring coefficients matrix; C_{vis} is the linearized viscous damping matrix; and $F(t)$ denotes time traces of the first-order wave exciting force that can be obtained through the fast Fourier transform algorithm of the frequency-domain results. In Eq. (10), the convolution term represents the memory effect of free surface induced by the radiation waves. In addition, $h(t-\tau)$, a retardation function, reflects the fact that the momentum change at time τ influences motions at current time t. According to the Ogilvie relation (Ogilvie 1964), the retardation function can be calculated from the frequency-domain hydrodynamic coefficients using the equation

$$h(\tau) = \frac{2}{\pi}\int_0^\infty b(\omega)\cos\omega\tau \mathrm{d}\omega = -\frac{2}{\pi} \times \int_0^\infty \omega[a(\omega) - a(\infty)]\sin\omega\tau \mathrm{d}\omega \tag{11}$$

where $a(\omega)$ and $b(\omega)$ are the added mass and potential damping coefficients at frequency ω, respectively. For the satisfactory asymptotic property of potential damping at both zero and high frequencies, the first term in Eq. (11) is normally chosen for calculation.

Considering the fully coupled hydrodynamic interactions between two vessels, the inertial term $[M + a(\infty)]$and convolution term $\int_0^t [h(t-\tau)]\ \{\ddot{\xi}(t)\}\ \mathrm{d}\tau$ can be expanded as Eq. (12)

and Eq. (13), respectively. Here, the first and second subscripts signify the suffered body and the induced body, respectively.

$$\begin{bmatrix} (M+a(\omega))_{11} & a(\omega)_{12} \\ a(\omega)_{21} & (M+a(\omega))_{22} \end{bmatrix} \begin{Bmatrix} \ddot{\xi}_1 \\ \ddot{\xi}_2 \end{Bmatrix} \tag{12}$$

$$\int_0^t \begin{bmatrix} h(t-\tau)_{11} & h(t-\tau)_{12} \\ h(t-\tau)_{21} & h(t-\tau)_{22} \end{bmatrix} \begin{Bmatrix} \ddot{\xi}_1 \\ \ddot{\xi}_2 \end{Bmatrix} \mathrm{d}\tau \tag{13}$$

2.4 High-Frequency Approximation

In the time-domain simulation, the accuracy of the retardation function is critical to obtaining satisfactory results without fluctuation and divergence with the advancement of time steps. The calculation of the retardation function requires the hydrodynamic coefficients to have a high truncation frequency. Nevertheless, the frequency-domain hydrodynamic code that is used to compute added mass and damping has its limitation in terms of the highest frequency that it can reach. According to Faltinsen (1990), the panel characteristic length must be less than 1/8th of the wave length for the accuracy of added mass and damping. Thus, a smaller panel size should be used for high-frequency solution as this can greatly increase the computing time.

$$b_{mm}(\omega) \to \frac{\beta'_{mm}}{\omega^2} \, (\omega \to \infty) \tag{14}$$

$$b_{mn}(\omega) \to \frac{\beta'_{mn}}{\omega^2} + \frac{\beta''_{mn}}{\omega^4} \, (\omega \to \infty), m \neq n \tag{15}$$

To avoid the high-frequency fluctuation of damping coefficients in Eq. (11), a simple but effective high-frequency approximation derived by Pérez and Fossen (2008) can be used. This method is based on the asymptotic property of damping coefficient. Note that Eq. (14) is used only for diagonal elements, whereas for non-diagonal elements, Eq. (15) is recommended for higher accuracy.

To better illustrate the calculation procedures of the time-domain simulation for multi-body cases, a flow chart (Fig. 2) is provided. Note that all the steps after diffraction analysis with HYDROSTAR (Bureau Veritas 2007) were completed by using the in-house program.

3 Numerical Simulation

Using HYDROSTAR, the numerical model is established in the frequency domain to calculate the hydrodynamic coefficients required in the time-domain simulation. For the focus on the hydrodynamic interaction effects induced by different wave directions, FLNG and LNGC float freely without any

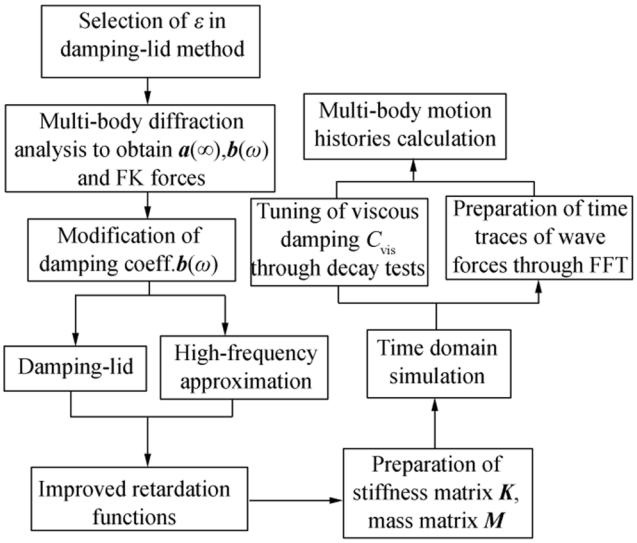

Fig. 2 Flow chart of the time-domain simulation

connector and fenders. The specific details of the two vessels are shown in Table 1. In the prototype, the gap width between vessels is 6 m.

The panel models of this side-by-side configuration are shown in Fig. 3. As can be seen, the gap zone is covered with red mesh grids because the application of damping-lid method entails the mesh of the gap free surface. The mesh area of the gap region is somewhat arbitrary and empirically defined, as explained by Shivaji and Sen (2016), which generally covers the major part of the gap along the parallel body of the LNGC. A fixed free-surface damping ε is adopted over the whole gap mesh following Watai et al. (2015); here, the value can be tuned through the gap wave elevations measured in the model tests following Chen (2011) (see Chapter 4.1.1).

The location of the side-by-side offloading is 300 m in depth. Wave directions from 135° to 225° are considered in the simulation. The radiation problems are solved to obtain the hydrodynamic coefficients from zero frequency to 3 rad/s. This is done in order to calculate the retardation function in the time-domain simulation. Moreover, diffraction problems

Table 1 Principal particulars of the FLNG vessel and the LNGC carrier

Designation	FLNG	LNGC
Length over all, L_{oa}/m	213.94	171.152
Breath, B/m	44.8	35.84
Depth, D/m	25.5	20.4
Draft, T/m	10.8	9
Displacement weight, Δ/t	98 923.1	52 821.3
Roll radius of gyration, R_{xx}/m	16	10.2
Pitch radius of gyration, R_{yy}/m	60	50
Yaw radius of gyration, R_{zz}/m	60	50

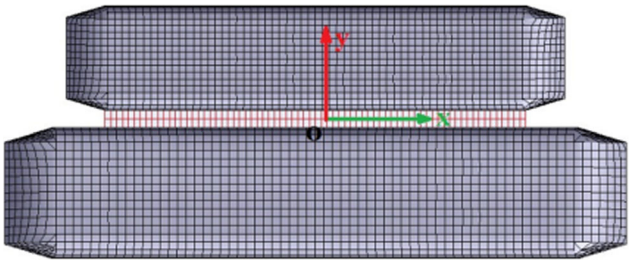

Fig. 3 Panel models of side-by-side configuration

under different wave directions are calculated for the wave exciting forces at discrete frequencies.

In the time-domain simulation, the viscous roll damping should be introduced for the simulation of realistic roll motions in oblique waves. Given that this study focuses on the influence of wave directions on the relative motions and not on the accurate prediction of roll motions, the roll damping of FLNG ($C_{vis}(4, 4)$) and LNGC ($C_{vis}(10, 10)$) in motion equation Eq. (10) is suggested to be estimated by linear damping in increments (5%–8%) of the critical damping (HYDROSTAR for Experts 2014). Hence, the approximated linear viscous damping is set as 5% of the critical damping for both vessels for safety considerations. The numerical roll decay simulation is then carried out to draw comparisons between the results with and without viscous damping (see Fig. 4). The natural periods of roll modes for the FLNG and LNGC are 13.08 and 11.22 s, respectively.

In addition, the lack of restoring forces for horizontal motions like the surge, sway, and yaw modes yields the numerical drifting divergence in the time-domain simulation for both vessels in oblique waves. Hence, the artificial spring model (Chen and Zhu 2010) is introduced to solve this problem. The restoring force and moment are calculated using the equation

$$Fr(x_1) = C_{\text{surge}}x_1, Fr(x_2) = C_{\text{sway}}x_2, Mr(x_6) = C_{\text{yaw}}x_6, \quad (16)$$

where the artificial restoring force coefficients for the surge, sway, and yaw modes are given by the following:

$$C_{\text{surge}} = k \cdot (\omega/2)^2 \cdot m, C_{\text{sway}} = k \cdot (\omega/2)^2 \cdot m, C_{\text{yaw}} = k \cdot (\omega/2)^2 \cdot I_{zz}, \quad (17)$$

where ω denotes the wave frequency, m denotes the mass of the body, and I_{zz} denotes the moment of inertia with regard to the yaw motion. In addition, k is a factor for tuning, where $k = 10$. All the artificial restoring force coefficients are incorporated into the stiffness matrix K in Eq. (10).

4 Results and Discussion

4.1 Hydrodynamic Coefficients

Through frequency-domain calculation, the modified hydrodynamic coefficients required for time-domain simulation are obtained, including the damping coefficients and the first-order wave exciting forces. The artificial damping ε is adopted to suppress the unrealistic resonance peaks in hydrodynamic coefficients. The wave exciting forces under various wave directions and the effects of high-frequency damping approximation are then illustrated.

4.1.1 Damping-Lid Method

By applying the artificial free-surface damping, unrealistic wave resonances can be suppressed, and the simulated energy dissipation facilitates a better convergence in the time-domain simulation (Watai et al. 2015) by avoiding the accumulation of trapped wave energy in the gap region. Determining the value of the damping factor is slightly arbitrary as no analytical guidance is currently available. Normally, this value is fixed by tuning the computed gap free-surface elevation with model test data or CFD calculation, which is extremely time-consuming. For many cases, the values of 0.02–0.05 are recommended for the damping factor ε (Pauw et al. 2007). In this study, three values (0, 0.02, and 0.05) are considered to calculate the free-surface elevation at the center point of the gap region, as shown in Fig. 5.

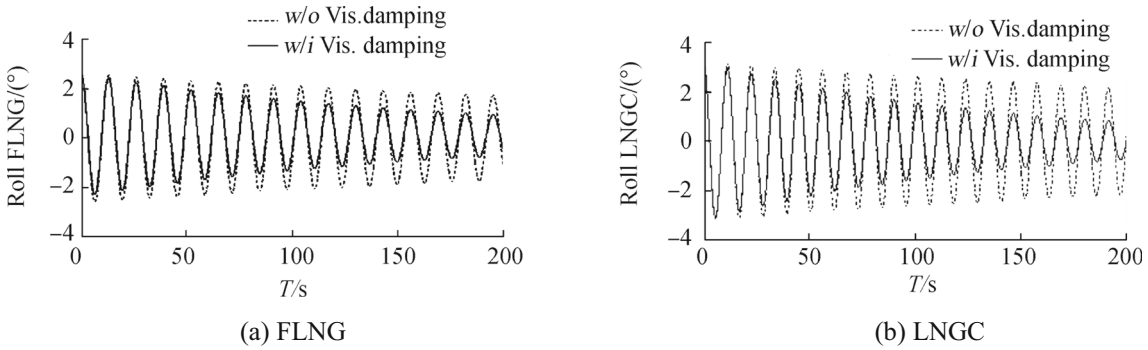

(a) FLNG (b) LNGC

Fig. 4 Numerical roll decay curves

As can be seen in Fig. 5, the increasing value of ε downplays the resonant peaks by about 50%, although this has a little effect on the non-resonance region. The first two peaks are more pronounced in revealing the concentration of wave energy at low-order resonant frequencies. The change of wave directions also influences the peak values, which are smallest under the 135° waves due to the strong shielding effects of the FLNG. For a comparable configuration, we take the value of $\varepsilon = 0.05$ following Qi (2011), who set the value as 0.042 with a gap width of 10 m in contrast to our 6 m gap (the higher value is used here because of a narrower gap). Note that the following time-domain calculation is based on frequency results calculated with $\varepsilon = 0.05$.

Based on the $\varepsilon = 0.05$, the free-surface elevation RAOs are also calculated when both the FLNG and LNGC are fixed, and these are represented by black lines in Fig. 5. As can be seen, the radiation waves induced by free-floating bodies have a significant influence on the low-order gap water resonances, which increase the resonant amplitudes and resonant frequencies of vessels in the fixed condition. The same phenomenon has also been captured by Shivaji and Sen (2016) under head seas.

4.1.2 Wave Exciting Forces

In the side-by-side offloading operation, sway exciting forces are significant in identifying the lateral motions and the gap width. Figure 6 shows the sway forces of two vessels in the side-by-side offloading under135/225° oblique waves, along with a comparison of these forces with those in the single-body case (dashed lines). Both the FLNG and LNGC suffer smaller sway forces at low frequencies ($\omega < 0.6$rad/s) compared with the single-body cases under any wave direction, indicating that the side-by-side configuration could minimize the wave forces similar to the sidewall effect. In addition, while at high frequencies, the gap water resonances greatly increase the wave forces. As shown in Fig. 5, the resonant frequencies of the wave forces concur with those of the free-surface elevation RAOs when both vessels are fixed.

The shielding effects are also obvious for wave forces. As shown in Fig. 6a for the FLNG, the wave directions' influence is complex, whereas in Fig. 6b for the LNGC, the sway force under 135° waves is uniformly decreased by the shielding of the large FLNG. This finding signifies the effective shielding capability of the FLNG to protect the LNGC under the135° waves.

4.1.3 Damping Coefficients

The quality of damping coefficients and the corresponding retardation functions is of great importance to the time-domain simulation. For the multi-body problem, the retardation function that is computed directly from the damping coefficients might fluctuate and decay slowly. Thus, improvements should be done to handle this problem, including the

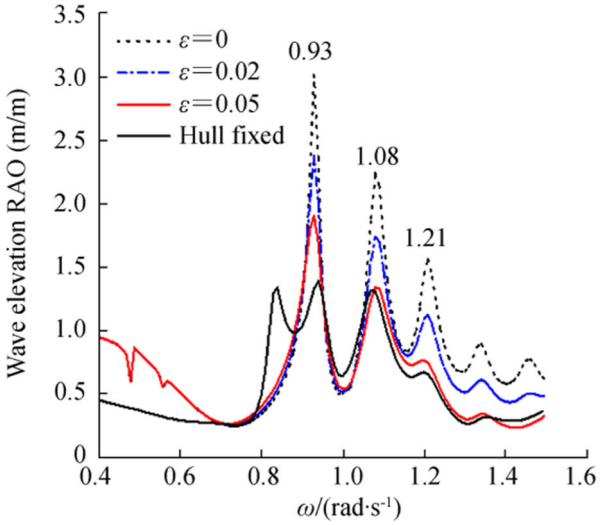

(a) 135°

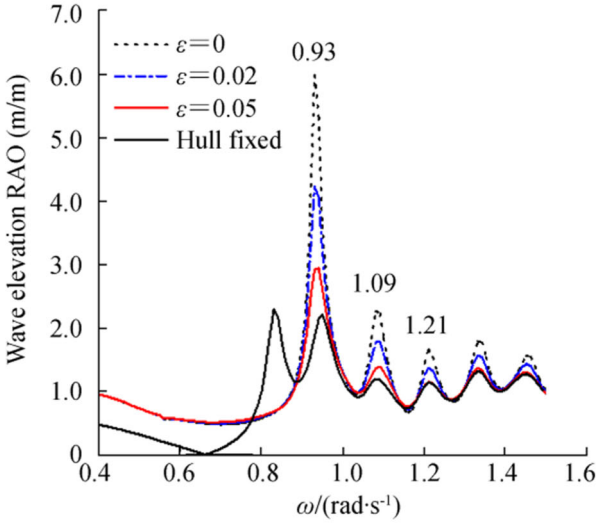

(b) 180°

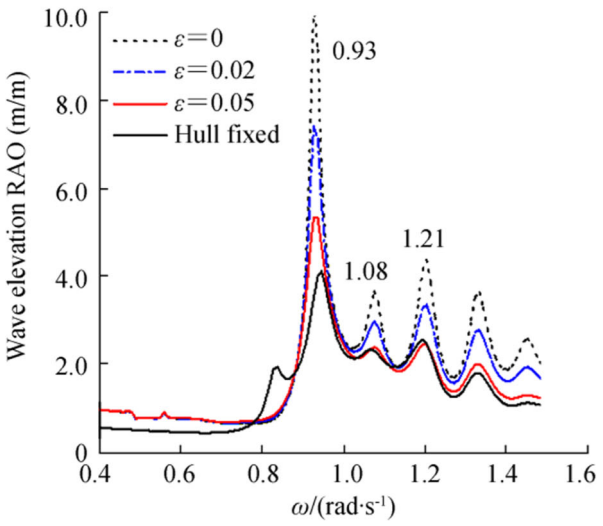

(c) 225°

Fig. 5 Free-surface elevation RAO at the center point of the gap region under the 135º, 180º, and 225° waves

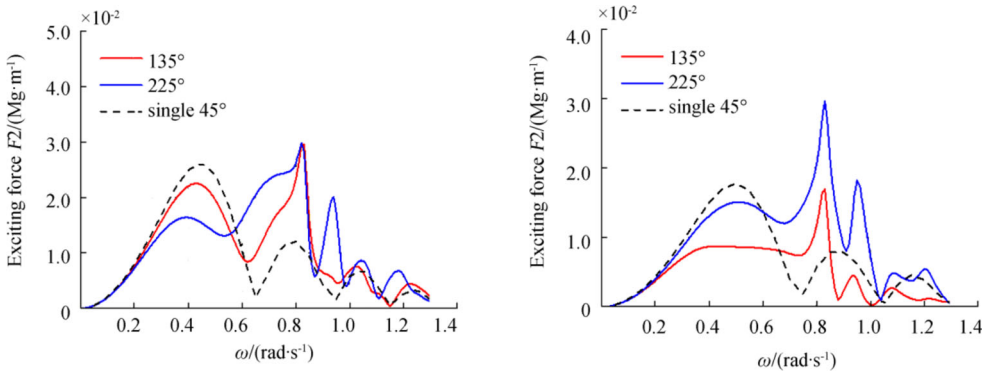

Fig. 6 Sway wave exciting forces of the FLNG and LNGC under different oblique waves ($\varepsilon = 0.05$)

use of the damping-lid method and high-frequency approximation.

Figures 7 and 8 show the damping coefficients and the corresponding retardation functions of the two modes for the FLNG. For the non-coupling (heave-heave) and coupling (surge-heave) mode, different methods of approximation are recommended in Chapter 2.4. As can be seen in Fig. 7, the non-zero ε serves to accelerate the decay speed of the retardation function to numerically simulate the energy dissipation. Furthermore, the high-frequency approximation (with the symbol: ext. (extension)) of the damping coefficient modifies the initial values of the retardation functions. In Fig. 8, the fluctuation of the damping coefficients at 2.5 rad/s is successfully smoothed by the high-frequency approximation, and the high-frequency components in the retardation function are filtered accordingly.

The damping-lid method helps suppress the unrealistic peak values of the damping coefficients and helps the retardation function decay faster. Meanwhile, the advantage of the high-frequency approximation is that it eliminates the fluctuation of the retardation functions and modifies the initial values. Note that the initial frequency for high-frequency approximation should be determined based on the relation between panel size and wave length

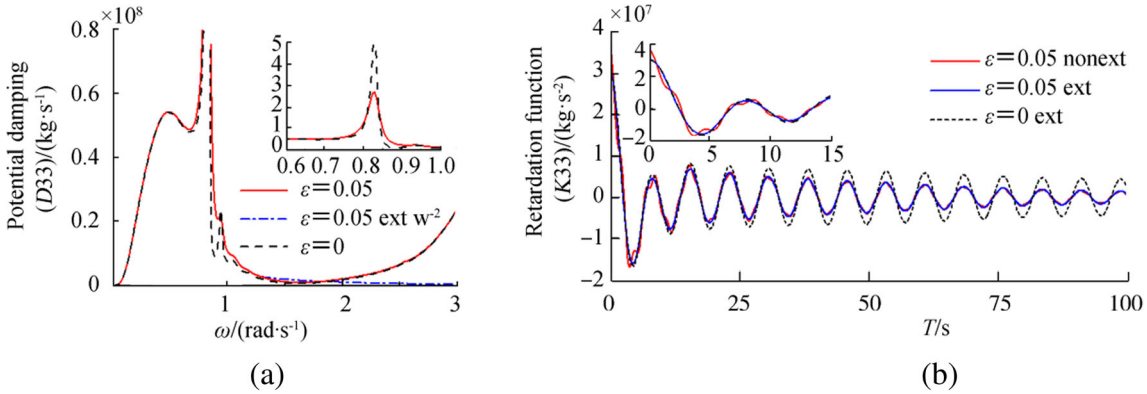

Fig. 7 Damping coefficients (**a**) and retardation functions (**b**) of the heave-heave mode for the FLNG

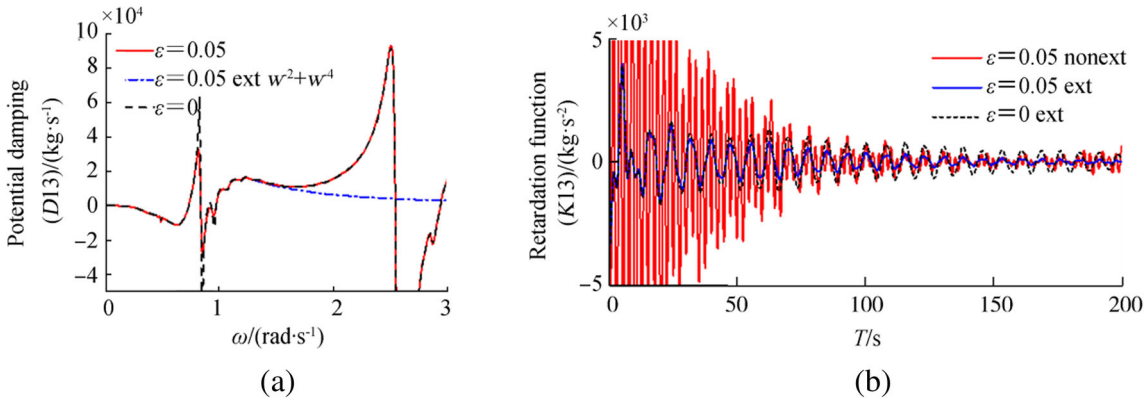

Fig. 8 Damping coefficients (**a**) and retardation functions (**b**) of the surge-heave mode for the FLNG

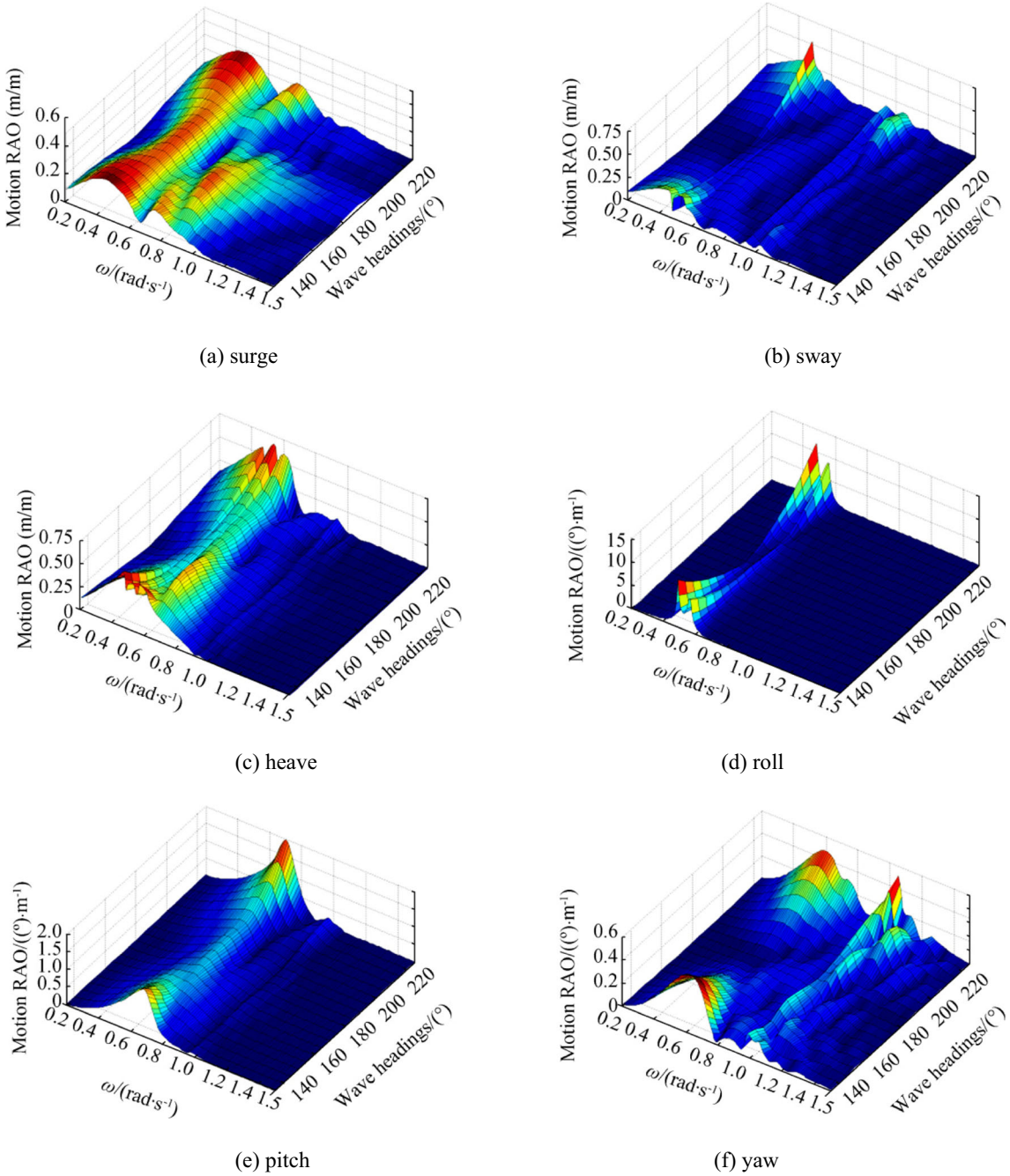

Fig. 9 Relative motion RAOs under 135°–225° waves

(the panel characteristic length must be less than 1/8th of the wave length, see Chapter 2.4).

4.2 Relative Motions under Oblique Waves

In order to analyze the influence of wave directions, relative motions are calculated by using the in-house code under the regular waves of different wave directions. The resonance phenomena of the relative motions bring high risks; thus, they are furthered studied in terms of the phase shifts and patterns of the gap free-surface resonances.

4.2.1 Relative Motion RAOs

The relative motions between the asymmetric side-by-side FLNG and LNGC under oblique waves are complex and more dangerous than those in the head seas. The time-domain simulations were carried out to obtain the steady-state motion responses of two vessels under successive wave directions from 135° to 225° and at discrete frequencies from 0.2–1.5 rad/s. This was done to better illustrate the changes of relative motions with the wave directions. The relative motion RAOs of all modes are plotted against the wave

directions and frequencies in Fig. 9. Here, we divide the frequency range into two parts, where the high-frequency region (0.9–1.2 rad/s) is featured by the gap water resonance (see Fig. 5), whereas the low-frequency region (0.2~0.9 rad/s) is dominated by hydrodynamic interactions.

Figure 9 shows that the low-frequency relative motions are generally symmetric with respect to the 180° waves (head seas), and then increase with the deviation of the wave directions from the head seas. For the sway, roll, and pitch modes, the relative motions tend to become intensified under wave directions approaching 225° when the LNGC encounters the incoming oblique waves. In the high-frequency region, we also observed that the gap water resonances give rise to the resonances of relative motions. Similarly, the high-frequency resonances of relative motions are also intensified under wave directions approaching 225°, especially for the sway and yaw modes. Therefore, the change of wave directions has a significant influence on the relative motions between the FLNG and LNGC, particularly for the transversal sway, roll, and yaw modes. Further, the 225° waves incoming obliquely from the side of the smaller LNGC tend to induce more violent relative motions.

4.2.2 Phase-Shift Effects

Given that the gap width is very sensitive to the transversal relative motions, the resonances of the sway, roll, and yaw motions are important in ensuring safety. Here, the phase-shift analysis is carried out to account for the phenomena. The phase shifts between the steady-state harmonic responses of the FLNG and LNGC are obtained from the time-domain simulation under regular waves. The absolute phase shifts are plotted against the wave directions and frequencies in Fig. 10. Note that the two vessels oscillate in the opposite directions (anti-phase motions) when phase shifts are closed to 180°; meanwhile, they oscillate in the same direction (in-phase motions) when phase shifts are closed to 0°.

In Fig. 10, the in-phase motions dominate the low-frequency region under most wave directions, except for the head seas when two bodies are side-by-side and are positioned symmetrically. For the roll mode (Fig. 10b), the phase shifts between two vessels are highly influenced by the wave directions at the frequencies between the resonant frequencies of the two vessels (0.48–0.56 rad/s). When the wave directions approach 225°, the phase shifts increase to 180°, so that the relative roll motions are correspondingly amplified (see Fig. 9) and become larger than those under 135° waves. Zhao et al. (2016, 2017) studied the roll resonances of LNG carriers and considered the internal sloshing in tanks, which might cause analogous phase shifts between the roll motion and sloshing loads.

Apart from the fact that roll resonances at two frequencies (0.48 and 0.56 rad/s) induce peak values of relative roll motions, the relative roll motions also tend to be amplified within

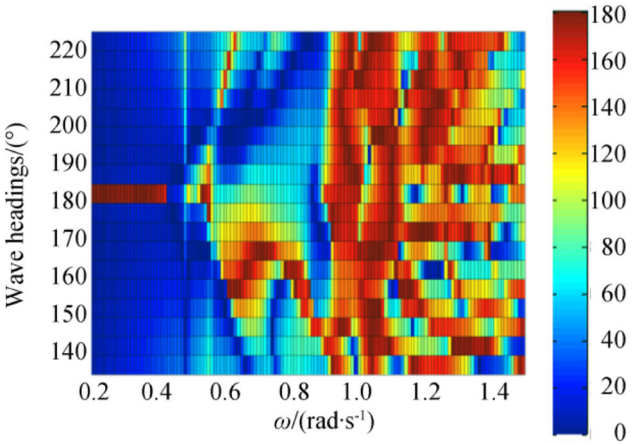

(a) Sway

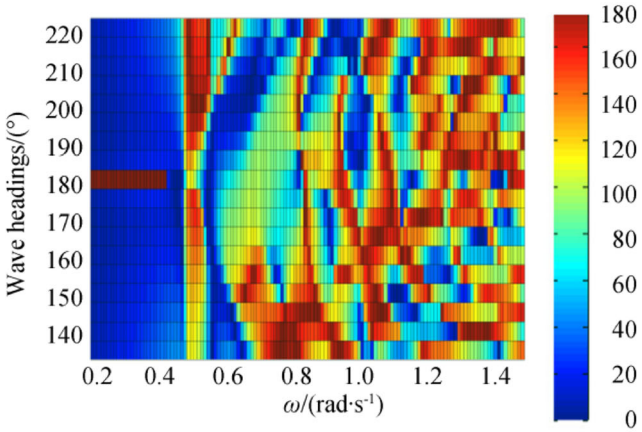

(b) Roll

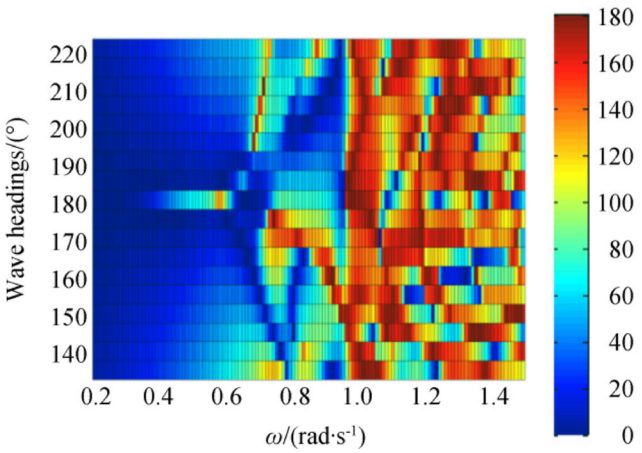

(c) Yaw

Fig. 10 Phase shift between the motions of FLNG and LNGC under wave directions from 135° to 225°

the span of two resonant frequencies where the wave energy is most likely to be concentrated. This brings about a higher probability of collisions. Figure 11 illustrates the time series of the roll motions of the FLNG and LNGC, as well as the relative motions, under 135°/225° regular waves at $\omega =$

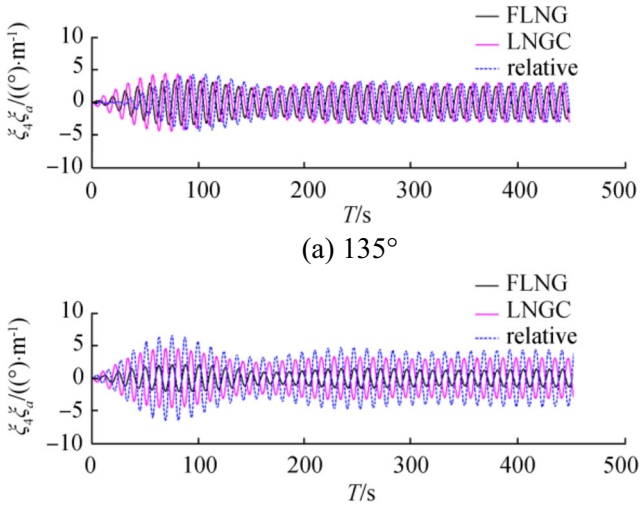

Fig. 11 Relative roll motion histories of the FLNG and LNGC under 135°/225° regular waves, $\omega = 0.52$rad/s

0.52rad/s(0.48rad/s < ω < 0.56rad/s). The results are non-dimensionalized by incoming wave amplitude (we only displayed the initial 450 s and above) for clarity. As can be seen, the relative roll motions under 225° waves are larger due to the anti-phase roll motions of the FLNG and LNGC, even when the roll motion of the FLNG is smaller, whereas the in-phase mode under 135° waves downplays the relative amplitude.

The transient effects of the roll motions are also noticeable before 250 s. For example, in Fig. 11b, the relative motion induced by the unit incoming waves reaches a maximum of 7.5° at 75 s, which is 1.5 times larger than the steady-state relative motion amplitude of 4°. Therefore, the abrupt enhancement of wave conditions should be examined for the risks of transient effects, especially coupled with anti-phase amplification of relative motions under 225° waves.

For the sway and yaw motions in Fig. 10, the phase shift of 180° (anti-phase mode) is predominant at the gap water resonance frequencies ($\omega > 0.9$rad/s) regardless of the wave directions. To better illustrate the influence of gap water resonance, the relative motion histories and instantaneous wave-elevation cloud maps are plotted at the gap water resonance frequencies in Figs. 12 and 13. In order to demonstrate the steady-state motions more clearly, only the results within a small time-window are shown.

In Fig. 12 where the wave frequency is 0.93 rad/s, corresponding to the first-order resonance (see Fig. 5), the longitudinal sloshing wave in the gap region is longitudinally symmetric with respect to the midship. The wave force induced by the sloshing waves would dispel two bodies apart and draw them back periodically, causing the anti-mode oscillation of the FLNG and LNGC in the sway mode. Note that under 135° waves, the incoming waves are better reflected by the weather-side FLNG to reduce the amplitude of sloshing waves of the gap. As a result, the relative motions are simultaneously suppressed.

Meanwhile, Fig. 13 shows the results in the yaw mode at the frequency 1.05 rad/s, which corresponds to the second-order resonance (see Fig. 5). Only the 225° wave condition

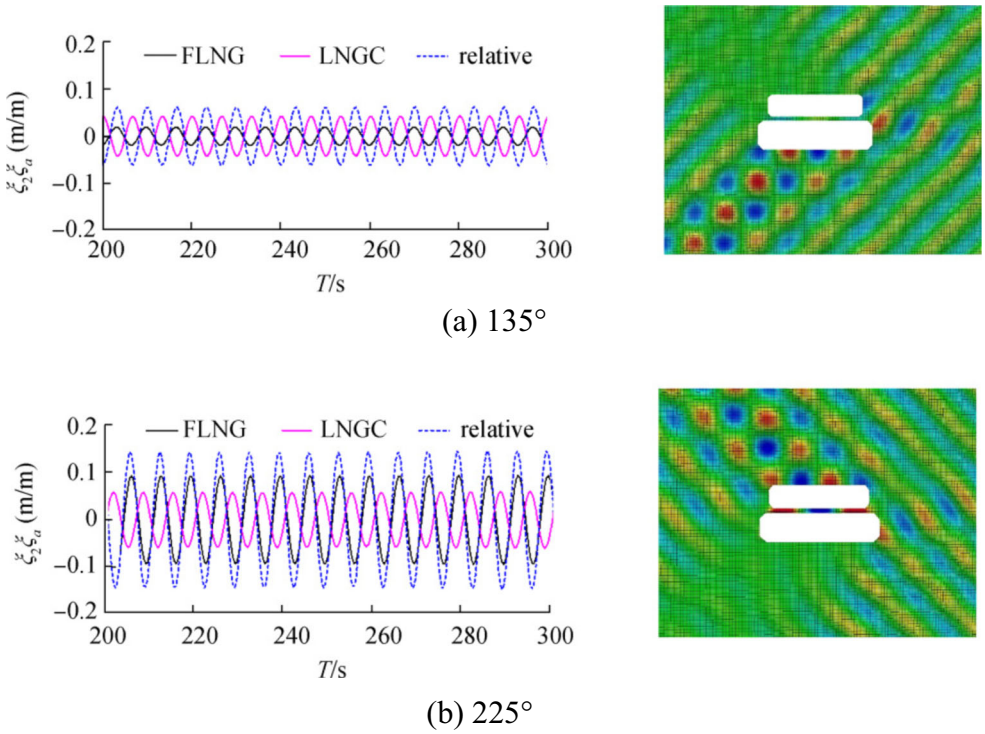

Fig. 12 Relative sway motion histories of the FLNG and LNGC and the instantaneous wave-elevation cloud map under 135°/225° regular waves, $\omega = 0.93$rad/s

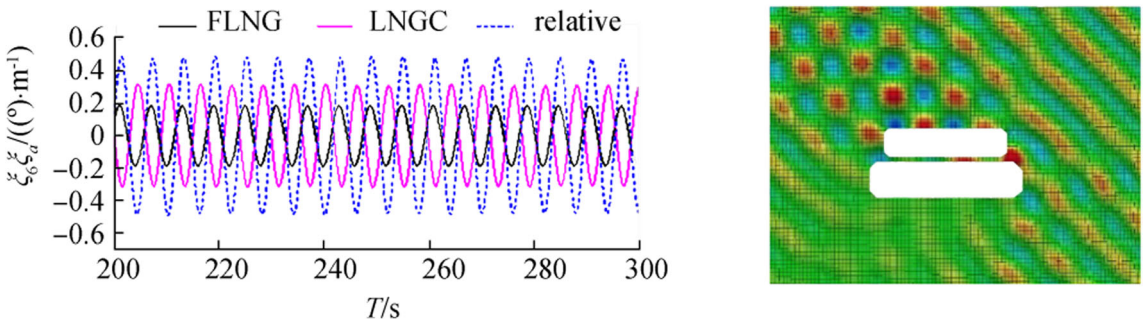

Fig. 13 Relative yaw motion histories of the FLNG and LNGC and the instantaneous wave-elevation cloud map under 225° regular waves, $\omega = 1.05$rad/s

is considered due to the stronger resonance of the relative yaw motion. As can be seen from the cloud map, the sloshing wave in the gap region is anti-symmetric with respect to the mid-ship, and this causes the moments in yaw modes for the FLNG and LNGC to display opposite directions.

In summary, the longitudinal symmetric sloshing modes in the gap region induce the resonances of the relative sway motions, whereas the longitudinal anti-symmetric sloshing modes cause the resonances of the relative yaw motions. The shielding effect of the FLNG under the 135° waves suppresses the resonances of both the gap waves and the relative motions.

5 Conclusions

Based on the modified hydrodynamic coefficients obtained with the aid of damping-lid method, this article uses the in-house code to carry out the time-domain simulation of side-by-side FLNG and LNGC under different wave directions. Several conclusions have been obtained, as discussed below.

1) Hydrodynamic coefficients, including wave exciting forces and damping coefficients, are analyzed prior to the time-domain simulation. The shielding effect of the FLNG can obviously reduce the sway wave forces acting on the LNGC. The modifications of damping coefficients by using the damping-lid method and the high-frequency approximation improve the quality of retardation functions and facilitate easier convergence for the time-domain equation solution.
2) Wave directions have a significant influence on the relative motions, particularly on the sway, roll, and yaw modes. Further, the 225° waves incoming obliquely from the side of the smaller LNGC tend to induce more violent relative motions.
3) Phase shifts are analyzed to account for the relative motion resonances. In the roll mode, when the wave directions approach 225°, the phase shifts between the resonant frequencies of two vessels (0.48–0.56 rad/s) increase sharply to 180°. The relative roll motions are accordingly agitated in the anti-phase mode. In addition, the amplified relative roll motions due to transient effect are particularly noteworthy under 225° waves.
4) In the sway and yaw modes, the phase shift of 180° (anti-phase mode) is predominant at the gap water resonance frequencies ($\omega > 0.9$rad/s) regardless of the wave directions. The sloshing modes of the gap water resonances are vital to the resonances of the relative sway or yaw motions. Nevertheless, the resonant amplitudes of both the gap waves and relative motions can be suppressed by the shielding effect of the FLNG under the 135° waves.

A further study will be carried out to consider the mechanical connections between the FLNG and LNGC, such as fenders and hawsers. In addition, a simulation for random seas or transient wave groups will be conducted to investigate the hydrodynamic performances of side-by-side FLNG and LNGC under real sea states.

References

Buchner B, van Dijk A, de Wilde J (2001) Numerical multiple-body simulations of side-by-side mooring to an FPSO, Proceedings of the 11th International Society of Offshore and Polar Engineers conference, Stavanger, Norway, 343–353

Bureau Veritas (2007) Hydrostar for experts user manual, Research Department of Bureau Veritas

Chen XB (2005) Hydrodynamic analysis for offshore LNG terminals, Proceedings of the 2nd Offshore Hydrodynamics Symposium, Rio de Janeiro, Brazil

Chen XB (2011) Offshore hydrodynamics and applications. The IES Journal Part A: Civil and Structural Eng 4(3):124–142. https://doi.org/10.1080/19373260.2011.595903

Chen JP, Zhu DX (2010) Numerical simulations of wave-induced ship motions in regular oblique waves by a time domain panel method. J Hydrodyn 22(5):419–426. https://doi.org/10.1016/S1001-6058(09)60230-4

Choi YR, Hong SY (2002) An analysis of hydrodynamic interaction of floating multi-body using higher-order boundary element method, Proceedings of the 12th International Society of Offshore and Polar Engineers Conference, Kitakyushu, Japan, 303–308

Cummins WE (1962) The impulse response function and ship motions. Schiffstechnik 9:101–109

Faltinsen OM (1990) Sea loads on ships and offshore structures. Cambridge University Press, New York

Fang MC, Chen GR (2002) The relative motion and wave elevation between two ships advancing in waves. Int Shipbuild Prog 49(3): 177–194. https://doi.org/10.1016/s0029-8018(00)00042-1

Fournier J R, Naciri M, Chen X B, 2006. Hydrodynamics of two side-by-side vessels experiments and numerical simulations, Proceedings of the 16th International Society of Offshore and Polar Engineers Conference, San Francisco, USA, 158–165

Huijsmans RHM, Pinkster JA, Wilde JJD (2001) Diffraction and radiation of waves around side by side moored vessels, Proceedings of the 11th International Society of Offshore and Polar Engineers conference, Stavanger, Norway, 406–412

HYDROSTAR for Experts (2014) User Manual. BUREAU VERITAS

Kim KH, Kim Y, Kim MS (2008) Time-domain analysis of motion responses of adjacent multiple floating bodies in waves, Proceedings of the 18th International Society of Offshore and Polar Engineers conference, Vancouver, BC, Canada, 301–307

Ogilvie TF (1964) Recent progress toward the understanding and prediction of shipmotions. In: 5th symposium on naval hydrodynamics, Bergen, 3–80 1964

Pauw WH, Huijsmans RHM, Voogt A (2007) Advances in the hydrodynamics of side-by-side moored vessels. Proc. of the 26th Offshore Mechanics and Arctic Engineering Conference (OMAE), San Diego, USA, 597–603. DOI: https://doi.org/10.1115/omae2007-29374

Pérez T, Fossen TI (2008) A derivation of high-frequency asymptotic values of 3D added mass and damping based on properties of the Cummins' Esquation. J Marit Res 5:65–78

Qi Q (2011) Hydrodynamic numerical calculation and analysis of FPSO-LNG multi-body system. Master thesis, Huazhong University of Science and Technology, Wuhan, 46–47. (in Chinese)

Sclavounos PD, Ma Y (2018) Wave energy conversion using machine learning forecasts and model predictive control. 33th international workshop on water waves and floating bodies, France

Shivaji GT, Sen D (2016) Time domain simulation of side-by-side floating bodies using a 3D numerical wave tank approach. Appl Ocean Res 58(2016):189–217. https://doi.org/10.1016/j.apor.2016.03.014

Soares CG, Taylor RE, Ewans K et al (2015) Safe offloading from floating LNG platforms. Appl Ocean Res 51:252–254. https://doi.org/10.1016/j.apor.2015.01.015

Van Oortmerssen G (1979) Hydrodynamic interaction between two structures floating in waves, Proc. 2nd Int. Conf. On behavior of offshore structures (BOSS'79), London, 339–356

Watai RA, Dinoi P, Ruggeri F, Souto-Iglesias A, Simos AN (2015) Rankine time-domain method with application to side-by-side gap flow modeling. Appl Ocean Res 50:69–90. https://doi.org/10.1016/j.apor.2014.12.002

Xu X, Yang JM, Li X, Xu LY (2015) Time-domain simulation for coupled motions of three barges moored side-by-side in floatover operation. China Ocean Eng 29:155–168. https://doi.org/10.1007/s13344-015-0012-4

Zhao WH, McPhail F (2017) Roll response of an LNG carrier considering the liquid cargo flow. Ocean Eng 129:83–91. https://doi.org/10.1016/j.oceaneng.2016.11.023

Zhao WH, McPhail F, Efthymiou M (2016) Effect of partially filled spherical cargo tanks on the roll response of a barge-like vessel. J Offshore Mech Arct 138(3):031601–0311-9. https://doi.org/10.1115/1.4032658

Zhao WH, Wolgamot H, Taylor PH, Taylor RA (2017) Gap resonance and higher harmonics driven by focused transient wave groups. J Fluid Mech 812:905–939. https://doi.org/10.1017/jfm.2016.824